Gawel, K., Todorovic, J., Liebscher, A., Wiese, B., Opedal, N. (2017): Study of Materials Retrieved from a Ketzin CO 2 Monitoring Well. - *Energy Procedia*, *114*, pp. 5799—5815.

DOI: http://doi.org/10.1016/j.egypro.2017.03.1718

Available online at www.sciencedirect.com

ScienceDirect

Energy Procedia 114 (2017) 5799 – 5815

Energy Procedia

13th International Conference on Greenhouse Gas Control Technologies, GHGT-13, 14-18 November 2016, Lausanne, Switzerland

Study of materials retrieved from a Ketzin CO_2 monitoring well

Kamila Gawel[a], Jelena Todorovic[a], Axel Liebscher[b], Bernd Wiese[b], Nils Opedal[a]*

[a]*SINTEFPetroleum Research, Trondheim, Norway*
[b]*German Research Centre for Geosciences, Potsdam, Germany*

Abstract

The Ketzin pilot site is the longest operating onshore CO_2 storage site in Europe. CO_2 injection began in June 2008 and ended in August 2013. In total five wells were drilled at the Ketzin pilot site. The Ketzin monitoring well 202 has been abandoned in autumn 2015. During the abandonment, well construction material samples were retrieved. The samples were retrieved from the cementitious plug as well as from the steel casing and the production string at different depths. The samples were analyzed by a set of complementary experimental techniques. The structure and macroporosity of cement samples were studied using X-ray computed tomography (CT) and scanning electron microscopy (SEM). The structural changes associated with hardening of the cementitious material downhole compared to the reference topside sample have been described. Casing and production string samples were studied using light optical microscopy to investigate microstructural changes resulting from CO_2 exposure. The relation between corrosion degree and the depth from which the samples were retrieved has been established.

Peer-review under responsibility of the organizing committee of GHGT-13.

Keywords: CO_2 storage; Ketzin; pilot; well cement; casing

1. Introduction

The Ketzin site is located in Brandenburg, Germany, (Fig. 1) and has been used for gas storage since 1964. The Ketzin pilot site is the longest operating onshore CO_2 storage site in Europe [1-5]. Research on CO_2 storage, led by German Research Centre for Geosciences (GFZ), started in 2004 within the framework of the EU project CO2SINK

* Corresponding author. Tel.: +47 982 86 641
E-mail address: Nils.Opedal@sintef.no

Peer-review under responsibility of the organizing committee of GHGT-13.
doi:10.1016/j.egypro.2017.03.1718

(2004-2010). Since 2004, the research and development activities at Ketzin pilot site have received funding from a number of German and EU projects, including for example CO2ReMoVe (2006-2011), CO2CARE (2011-2013), CO2MAN (2010-2013) and the ongoing project, COMPLETE (2013-2018). The COMPLETE project focuses on the post injection and closure phase, where the objectives are:

- For the first time ever close the complete life-time cycle of a CO_2 storage site at pilot scale.
- Expand knowledge on post-injection and post-closure monitoring and long-term site behavior.
- Provide first-hand experiences on site abandonment and transfer of liability.

CO_2 injection began in June 2008 and ended in August 2013. During this period, an amount of about 67 kilotons of CO_2 was injected into a saline aquifer at depths of 630 m to 650 m. Five wells were drilled at Ketzin pilot site as presented schematically in Fig. 1. Well Ktzi 201 was a combined injection/observation well, while wells P300 (~ 450 m), Ktzi 200 and Ktzi 202 (750 m - 800 m), and Ktzi 203 (~ 700 m) were completed for monitoring. The Ketzin well 202 was abandoned in autumn 2015. The various materials (cement, casing, production string) were retrieved from several different depths during the abandonment operation.

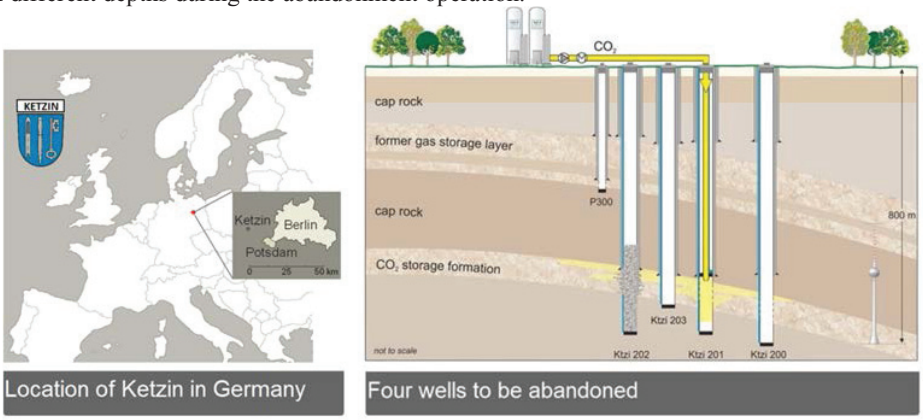

Fig. 1. Location of Ketzin and schematic illustration of Ketzin wells.

Besides the Ketzin site, there is a number of operative and planned pilot CO_2 storage projects around the world, as for example Weyburn-Midale in Canada, Lacq in France, Otway in Australia and Hontomin in Spain. However, to the best of our knowledge, none of the pilot CO_2 storage projects have reported retrieval and characterization of downhole samples. Retrieval of downhole samples has neither been reported for the well-known CO_2 injection sites such as Sleipner, Snøhvit and In-Salah [6]. There has been only a few reports [7-9] on characterization of the cement and steel field samples after being exposed to downhole conditions. Carey et al. [7] studied core samples consisting of casing, cement and shale caprock recovered from a 55-year old well from the SACROC field where CO_2-EOR operations had been going on for more than 30 years. Crow et al. [8] conducted an investigation of integrity of a 30-year old well from a natural CO_2 production reservoir. In this study, core samples consisting of casing, cement and formation, were recovered at depths ranging from within the CO_2 reservoir to about 70 m above the reservoir, in the caprock. Scherer et al. [9] investigated the condition of the cement prior to CO_2 injection. In this work, cement samples were recovered at different depths from a 19-year old well from the Teapot Dome oil field. The common observation in these field studies was that the cement has experienced some degree of alteration and/or degradation due to exposure to CO_2 brine [7, 8], or reaction with the surrounding formation [9].

Compared to the previous field studies, the Ketzin site is much "younger", but has an advantage of being a pilot site designed for extensive research. This work is a continuation of the study from 2014 [10] focusing on the topside pipelines used for injection of CO_2. The cement, casing and production string samples retrieved from the Ktzi 202 well were the first batch of downhole samples that have been studied, and more samples will be retrieved from the other wells in the next abandonment stage. The objectives of this work with respect to material characterization were to study:

- Changes in micro-structure and porosity of cement samples in respect to topside sample
- Surface topography of corroded casing/ production string samples

Characterization methods used were X-ray micro-computed tomography (CT), scanning electron microscopy (SEM) combined with energy-dispersive X-ray spectroscopy (EDX), and optical microscopy. These methods have been selected as the most appropriate with respect to the quality, type and sizes of the received cement and steel samples. A remark has to be made that cement used for the construction of the well Ktzi 202 was a commercially available product thus, no detailed quantitative compositional analysis of the cement samples was permitted. The structure and macro-porosity of cement samples was studied by CT, and micro-structure by SEM/EDX. Casing/production string samples were studied using optical microscopy. Inner and outer surfaces of casing and production string samples extracted from different depths were compared.

2. Experimental

2.1. Samples from Ketzin well 202

2.1.1. Cement samples

The cement plug was set into the well in 2013. Cement plug samples of the top most part of the plug were cored in 2015 at a depth interval of 521 - 523 m. Sample of the same material cured at ambient conditions (atmosphere pressure and room temperature) was used as a reference. Figure 2 presents the cored cement plug cylinders from Ktzi 202, as received from GFZ and after further sample preparation for CT and SEM studies. It is reasonable to assume that none of these cement samples have been in contact with CO_2.

The samples were analysed as received using X-ray computed tomography (CT). After the samples were analysed using CT, smaller cores (~1 cm in diameter) were drilled out and used in SEM/EDX analysis. One topside (reference) and one downhole sample (521 m) were analyzed. Descriptions of CT and SEM/EDX analyses are given in section 2.2.

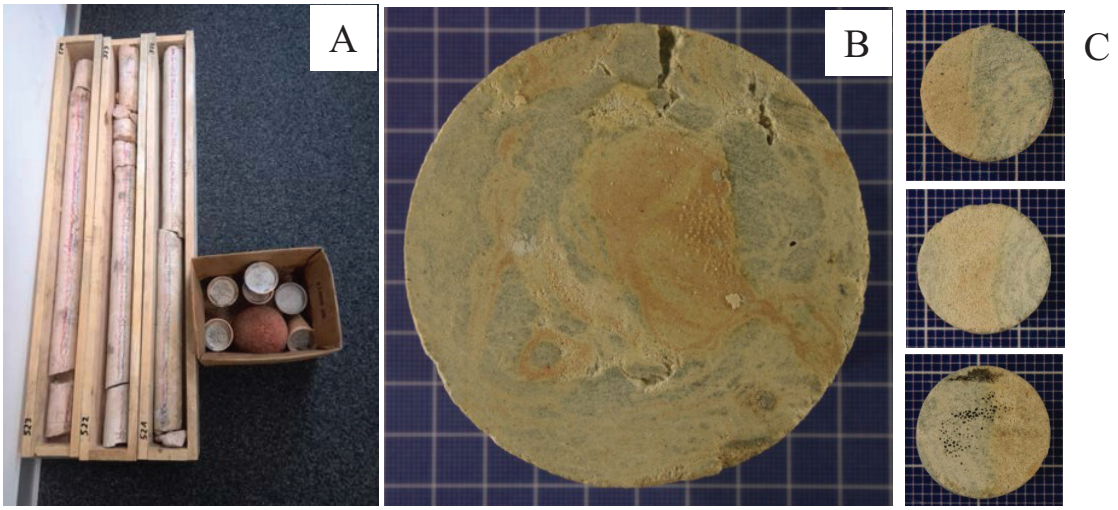

Fig. 2. (a) Core samples from Ktzi 202. (b) Example: surface of cement core from depth of 521 m. (c) Small cement cores drilled for SEM analysis from sample retrieved at depth of 521 m, not to scale with (b).

2.1.2. Casing samples

Three casing and three production string samples from Ketzin 202 well were analyzed. The casing was made of steel grade L80 13 Cr of original thickness 9,2 mm, and the production string was made of steel grade K55 with original thickness of 8,9 mm. Casings had the external diameter of 9-5/8" and production strings of 5-1/2". Samples were retrieved by coring at six different depths measured from topside. The retrieval depth of each sample is shown in the Table 1. Figure 3 shows how the Well Ktzi 202 was constructed and helps to localize the area in the well from which the samples were taken. All the samples were circular with a diameter of 55 mm.

The samples were cored about one month after the pipes were pulled from the wellbore, and additionally the pipes were lying unprotected on the ground. Thus, the pipes were in contact with rain and sun in the period of July-August. It is likely that this exposure might affect the exterior of the pipes, the level of corrosion from this exposure has not been quantified. Though, considering the weather conditions in Brandenburg, Germany, compared to the downhole conditions, it is assumed that the corrosion due to this unprotected exposure was negligible.

Production string samples have been in contact with CO_2 from the beginning of 2009 until the first stage of cementation in 2013 [5]. Casing samples have most likely never been in contact with CO_2.

In order to capture macroscopic differences between samples, the samples were first photographed using an ordinary Pentax K20 photographic camera equipped with SMC Pentax 16-45 mm lens.

Microscopic images of internal and external surfaces of two representative samples, namely T9 and C19 (see Table 1), were taken using stereo microscope Leica M420 equipped with Leica DFC420 camera and fiber optic illuminator Volpi Intralux 5000.

Two methods have been used to estimate the thickness of the rust layers at surfaces of casing and production string samples: (1) Mitutoyo digital dial indicator (accuracy 0.001 mm) was used to measure distance between the top of the rust layer and the plain metal surface from which the rust layer was removed using a sand paper. This method was applied to validate thickness of internal rust layers. The values presented in this paper are average values based on four measurements. (2) Optical method relying on measuring average thickness based on optical microscopy image: This optical method was applied to two casing and production string samples (T9 and C19). The samples were first cast in an epoxy resin in order to preserve the rust layer from mechanical damage, then cut, polished and imaged using a stereo microscope. Average thickness of the rust layer was estimated based on distance measurements on the image using ImageJ freeware software. The thickness values of rust layers were quite scattered along the cross-section and the average thickness was estimated based on 13 measurements. Standard deviations from the average value have been estimated.

Table 1. List of casing/production string samples cored from Ketzin 202.

No.	Name	Casing	Depth (m)
1	T452	5-1/2´´	452.2
3	T229	5-1/2´´	228.5
5	T9	5-1/2´´	8.8
7	C246	9-5/8´´	245.8
9	C115	9-5/8´´	114.7
11	C19	9-5/8´´	18.8

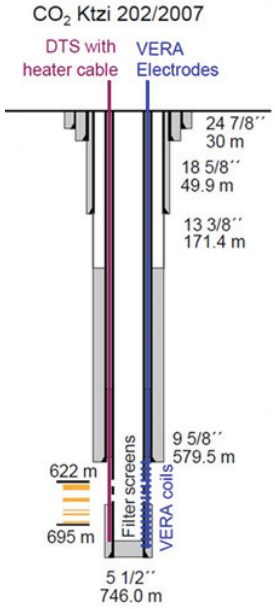

Fig. 3. Schematics of the well Ktzi 202, adapted from reference [5].

2.2. Characterization Methods

2.2.1. X-ray Computed Tomography

X-ray computed tomography (CT) was used to analyze and visualize the cement cores in 3D. In this study we used an industrial CT scanner XT H 225 ST, located at NTNU Institute of Physics. The CT was operated at 220 kV and a current of 120 µA, and scanning was performed with a tin filter. After reconstruction of the raw CT data, 2000 cross sectional slices (2000×2000 pixel) were obtained per dataset. Exception was the reference cement sample, which was shorter than downhole samples, which resulted in 1116 slices.

2.2.2. 3D reconstruction in Avizo software

The cross sectional CT slices were then analyzed and reconstructed into 3D volumes in AVIZO Fire 9.0 software (FEI Visualization Sciences Group). Subsets of representative CT slices were selected for each sample, as shown in Table 2. Several hundreds of slices at the ends of the cores, where the cement was damaged or incomplete, were disregarded from analyses in Avizo. The segmentation procedure depends on the complexity of a dataset. Cement material was typically segmented by using intensity threshold, paintbrush and/or magic wand tools. Due to image intensity differences between the CT datasets, a different default threshold range for cement bulk was obtained for each CT data set, as listed in Table 2. After the initial segmentation, the cement-label contained both cement bulk and void/ leakage paths voxels. 3D smoothing (level 3) of the labels was run after defining cement bulk in order to obtain smooth cement surface in 3D visualisation.

There were observed heterogeneities within the cement material. These heterogeneities were distinguished from the cement using a threshold tool with ranges listed in Table 2. They will be further referred to as "a second material" or "material 2". The greyscale values for cement bulk and the second material were overlapping significantly, resulting in low contrast between them. The selected threshold values resulted in partial extraction of the second material, and hence cannot be used for volume quantification, but only for visualisation in 3D. The defects (e.g. voids and cracks) and potential leakage paths within the cement were defined using threshold, magic wand and paintbrush tools from the previously defined cement. Porosity values for all samples were calculated from

label volumes from the material statistics extracted in Avizo. Porosity was obtained as a ratio of void/ leakage paths volume and total core volume (cement, the second material and voids/leakage paths).

Table 2: Intensity threshold ranges used for segmentation of cement bulk and the second material.

Cement core	Analysed CT slices	Cement threshold	Material 2 threshold
Reference sample	221 - 871	15 - 180	none
521 m	381 - 1380	11 - 434	40 - 434
522 m	301 - 1700	14 - 254	35 - 254
523 m	426 - 1425	11 - 211	45 - 211

2.2.3. Scanning Electron Microscope

For SEM/EDX study, Table Top SEM Hitachi TM3000, located in the NTNU NanoLab Cleanroom was used. This microscope operates at 5 kV and 15 kV in backscattered electron mode (BSE). BSE images were taken at 5 kV, whereas EDX analysis was performed at 15 kV. This SEM is equipped with an EDX detector which gives 2D mapping (elemental images) and total EDX spectrum over the mapped area. The EDX spectrum provides qualitative characterization of the elements present in the sample. However, no reliable quantitative estimation of the amounts of different elements is possible in this instrument for complex samples such as cement. The received cement core samples were drilled to obtain small cores (about 10 mm in diameter, Fig. 2 (c)) which were further cut into thinner discs to fit onto the sample stage. The heterogeneities visible by eye in the original downhole cement cores were also present in the small sections, and this was particularly studied in SEM.

3. Results and Discussion

3.1. Cement cores

3.1.1. CT Characterization of Cement Cores

Representative reconstructed CT images for the reference sample and downhole cement core samples are shown in Fig. 4. The CT image quality was sufficient to reconstruct void and leakage paths network and heterogeneities in the bulk cement. 3D visualisation of cement core volumes depicting distribution of voids and heterogeneities (second material) is shown in Fig. 5. The reference sample had rather homogeneous cement bulk with micro-sized closed pores evenly distributed in the whole sample volume. The downhole samples were heterogeneous – two distinguishable materials were observed within the cement volume in addition to voids and leakage paths. This heterogeneity was also visible on sample surfaces, as shown in Fig. 2. All the downhole cement cores contained a mixture of at least two different materials: unaltered cement (greyish in Fig. 2, and darker in CT images Fig. 4) and reacted/altered cement (yellowish in Fig. 2, and brighter in CT images Fig. 4). As the reference cement sample, cured directly after blending, was homogeneous in contrast to the downhole samples, the heterogeneity has to be ascribed to the downhole history of the cement slurry that could possibly encompass mixing with other fluids present in a well during cementing or during/after curing.

The cement core samples represent the uppermost 3 m of Stage 1 cementation of Ktzi 202. After placing the cement plug but before the cement hardened, well Ktzi 202 was filled with brine, so the inhomogeneities present within samples can possibly arise from contact of the slurry with the brine. At least two effects have to be considered while looking for possible explanations for the yellowish/altered cement. First, potential contact of the cement plug with CO_2 and possible carbonation has to be discussed. In a study of oil well cement samples from the SACROC unit, an "orange zone" in the cement was observed [7]. It was concluded that the "orange zone" originated from cement carbonation upon reaction with brine-CO_2. Given that the analysed samples constituted the uppermost part of the plug and that the cement used was CO_2 resistant the carbonation scenario is rather unlikely. Another reason of the visible cement alteration could be dissolution of rust in the brine placed over the cement slurry and its mixing with the slurry. EDX studies presented later in this section suggest that the altered cement material contained larger amounts of NaCl that strengthens the brine mixing hypothesis. In order to unequivocally answer the question

about the origin of the yellowish/altered cement material a detailed quantitative compositional analysis of the cement samples would be required. This however, was not permitted as the cement used for the construction of the well Ktzi 202 was a commercially available product.

A rough estimation of volume of macroscale pores (porosity) was done for all samples based on AVIZO analysis of CT data. Any millimetre-scale defects (like voids, closed pores, cracks etc.) present in cement bulk contributed to this value. Due to limited resolution of CT images, using intensity threshold in Avizo to distinguish voids and leakage paths from the cement it is to some degree a subjective method of image segmentation and thus cannot be treated as a quantitative. Especially for lower resolution of CT images, a small increase or decrease of threshold usually results in large change in pore volume, directly affecting calculated porosity values. This was the case for the cement samples analysed in this report. Thus, three different threshold ranges (Table 3) were selected to obtain an overview of porosity depending on the method applied. The obtained porosity values for all samples are presented in Table 3. Threshold range (0-23) can be regarded as a minimum to extract voids/ leakage paths, whereas (0-27) resulted in significant increase in voids/ leakage paths volume and increased connectivity of the voids. Thresholds larger than (0-27) selected significant portions of cement bulk volume as well, which would have resulted in an overestimation of porosity.

The core from a depth of 522 m had the lowest porosity for the minimum threshold range (0-23) and no correlation between location/depth and pore volume was observed. The lowest threshold range was used for 3D visualisation in Fig. 5. Significant volumes of voids are present in the cores from depths of 521 and 523 m. Increase of threshold resulted in increase of porosity for all samples. However, for threshold (0-27) there is less difference in porosity values between the samples. The overall estimated porosity is thus within a range of 1-6 %.

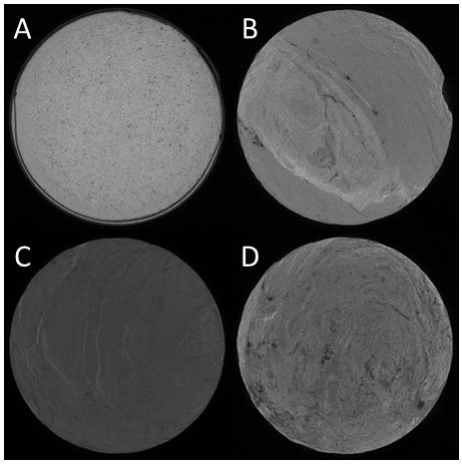

Fig.4. Representative reconstructed CT images for: (a) reference sample cured at ambient conditions; and downhole cement core samples taken from depths of (b) 521 m, (c) 522 m, and (d) 523 m.

Table 3. Porosity and leakage paths in % of total core volume calculated from the reconstructed CT volumes for three different threshold ranges for voids/leakage paths.

Cement core	Porosity & leakage paths (core volume %)		
	Threshold range (0-23)	Threshold range (0-25)	Threshold range (0-27)
Reference sample	0.8 %	2 %	5.7 %
521 m	0.8 %	1.4 %	4.3 %
522 m	0.13 %	0.74 %	6 %
523 m	1.5 %	2.7 %	5.4 %

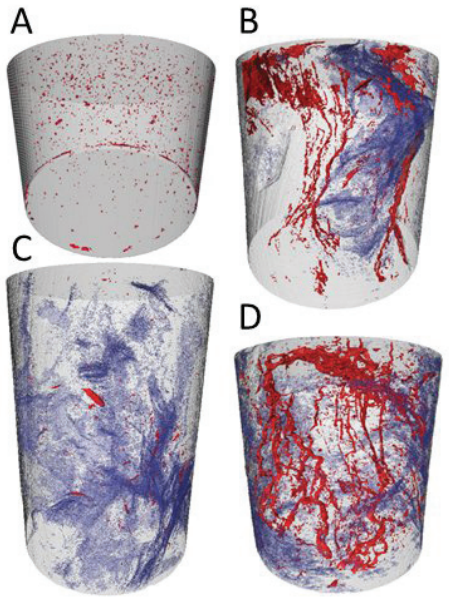

Fig. 5. 3D visualisation of cement core volumes: (a) reference sample cured at ambient pressure and temperature; and downhole samples taken from depths of (b) 521 m, (c) 522 m, and (d) 523 m. Cement volume is presented in grey color, voids/ leakage paths- red, and the second material - blue.

3.1.2. SEM Characterization of Cement Cores

BSE images of the reference cement sample drilled from within bulk are shown in Fig. 6. Sample surface was rather rough (no polishing was done before SEM) with grains of various sizes. EDX mapping of a smaller region of interest taken from the area shown in Fig. 6 (b) is presented in Fig. 7: BSE image and EDX elemental maps for some of the most abundant elements. The EDX spectrum shown in Fig. 8 is the total spectrum taken from the region of interest in Fig. 7. The main elements present in the cement sample were: Si, O, Ca, Na, Cl, Mg, Al and C. EDX analysis indicated that the distinct particles found on the surface contained mainly silica, and were surrounded by Ca rich bulk.

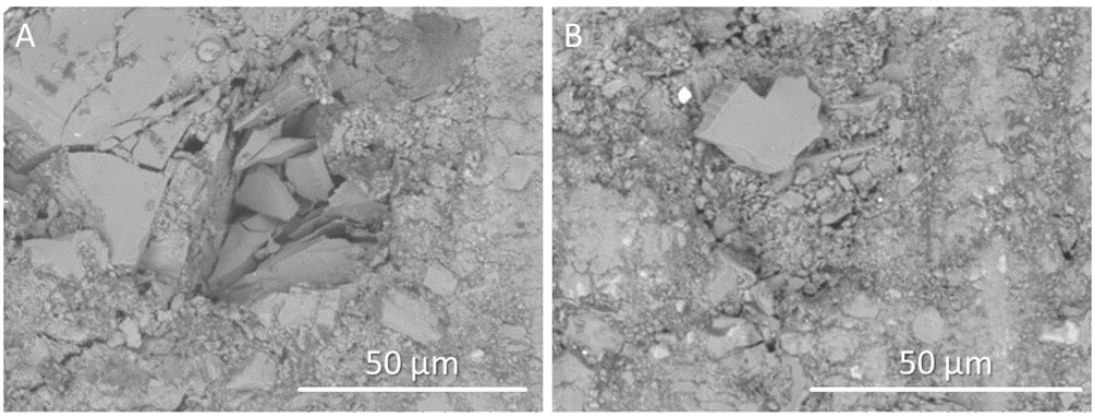

Fig. 6. Overview BSE images of the reference sample (cement plug cured at atmosphere pressure and temperature during cementing operation).

The 3D reconstruction of CT datasets revealed that the downhole cement samples were heterogeneous. The cement core from a depth of 521 m contained the most distinct distribution of different materials, as seen in Figs. 2 (b,c) and 5 (b). Thus small cement cores, containing both materials distinct greyish and yellowish regions in Fig. 2 (b), were drilled only out of this core for SEM study (Fig. 2 (c)). Overview BSE images of the bottom most cement core in Fig. 2 (c) are shown in Fig. 9. This small core was selected since it happened to be well divided in the middle into the two distinct materials. The boundary between the two materials is clearly visible in the BSE images both at the lowest magnification (Fig. 9 (a)) and upon increase of magnification (Fig. 9 (b)). The "bright" right half of the sample contains a mixture of "bright" bulk material and "dark" grains which may have originated from the "dark" phase in the left half.

The EDX mapping was performed along the boundary at several locations, as well as on both sides of the boundary – within the two distinct materials. EDX results from all these different regions were consistent, and representative EDX characterization of the 521 m sample is shown in Figs. 10 and 11. BSE image of a region of interest across the boundary, and EDX elemental maps for some of the most abundant elements are presented in Fig. 10. Ca, Si and O were most abundant on the left half, whereas Na and Cl were dominant on the right half of the sample. The boundary in EDX maps between Ca and Si rich, and Na and Cl rich regions is following the boundary seen in the BSE image (Fig. 10). However, the boundary between the two distinct materials is not as clear in 15 kV BSE (Fig. 10) image as in 5 kV BSE (Fig. 9) due to reduced surface sensitivity to the electron beam with voltage increase.

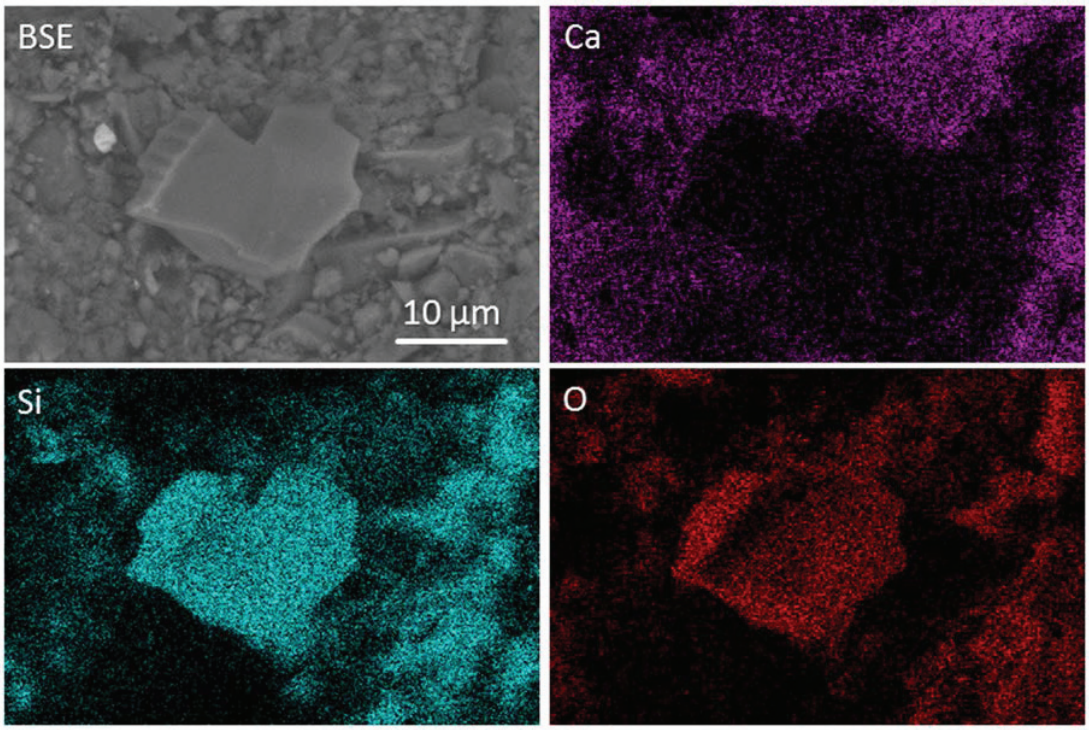

Fig. 7. BSE image of the reference sample surface and EDX elemental maps for the most abundant elements: Ca, Si and O.

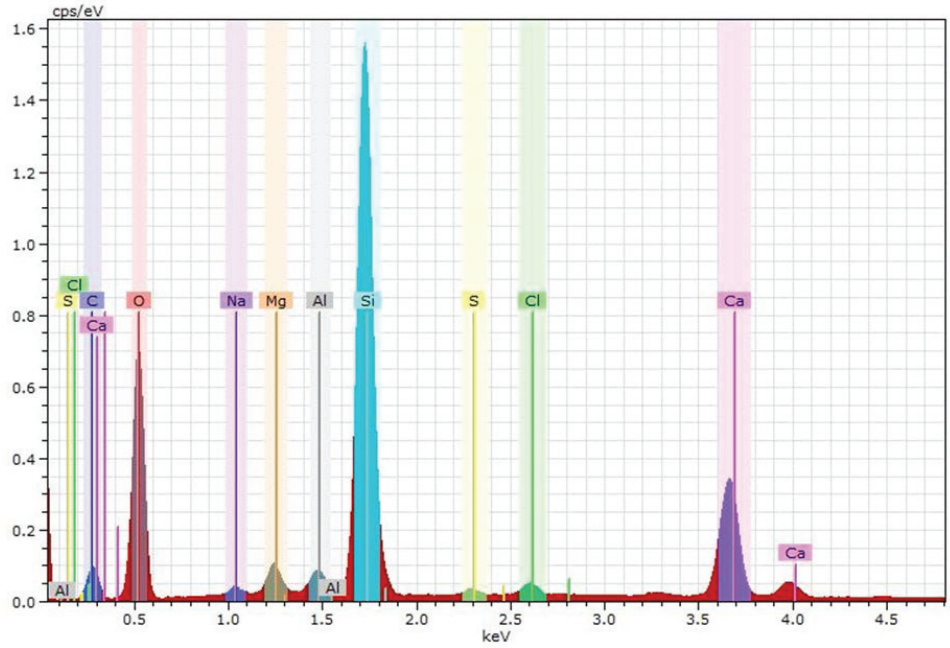

Fig. 8. Total EDX spectrum from the region of interest shown in Fig. 7; normalized counts per second versus energy (eV) of the detected X-rays.

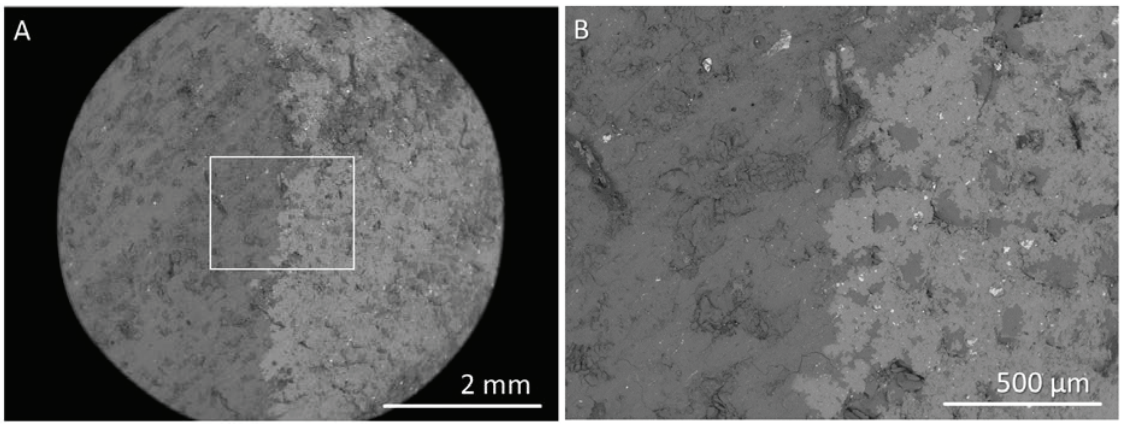

Fig. 9. BSE images of (a) surface of the cement plug from a depth of 521 m. (b) the region marked by the rectangle in (a) – showing boundary between the two materials, where grey cement is on the left side, and yellow material on the right.

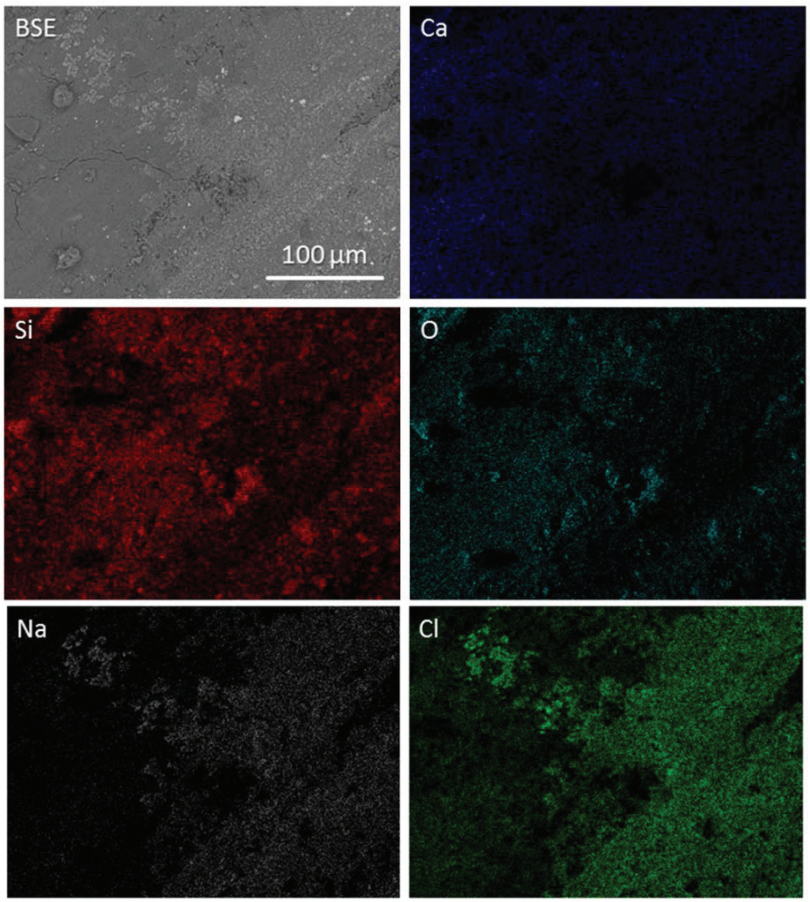

Fig. 10. BSE image of the downhole cement (521 m) surface and EDX elemental maps for the most abundant elements: Ca, Si, O – on the left half, and Na and Cl – on the right half of the sample.

The EDX spectrum shown in Fig. 11 is the total spectrum taken from the region of interest shown in Fig. 10. The elements detected in this region of interest were: Si, O, Ca, Na, Cl, Mg, Al, S, Ti and C. Although EDX spectrum of the reference sample also contained Na and Cl, ratio of the counts per seconds for Si and Na (or Cl) was higher for 521 m sample. All elements present in the EDX spectrum in Fig. 11 were found in all scanned regions of interest on both sides of the boundary. Comparing counts per second for each present element, confirmed that Na and Cl were dominant on the "bright" right side, whereas Si, Ca and O were more abundant on the "dark" left side of the sample. EDX mapping (not shown) also indicated that the "dark" grains mixed with the bulk on the left side contained silica (as in the reference sample).

EDX analysis thus indicated that the downhole cement samples contained salts (NaCl and possibly other) which were mixed with Ca-Si-O cement matrix. This finding can be correlated with visual observations (yellowish material as seen in Fig. 2 (b,c)) and CT results (heterogeneities present in all downhole samples). The presence of salt most likely was a result of filling the well with brine after the cement placement.

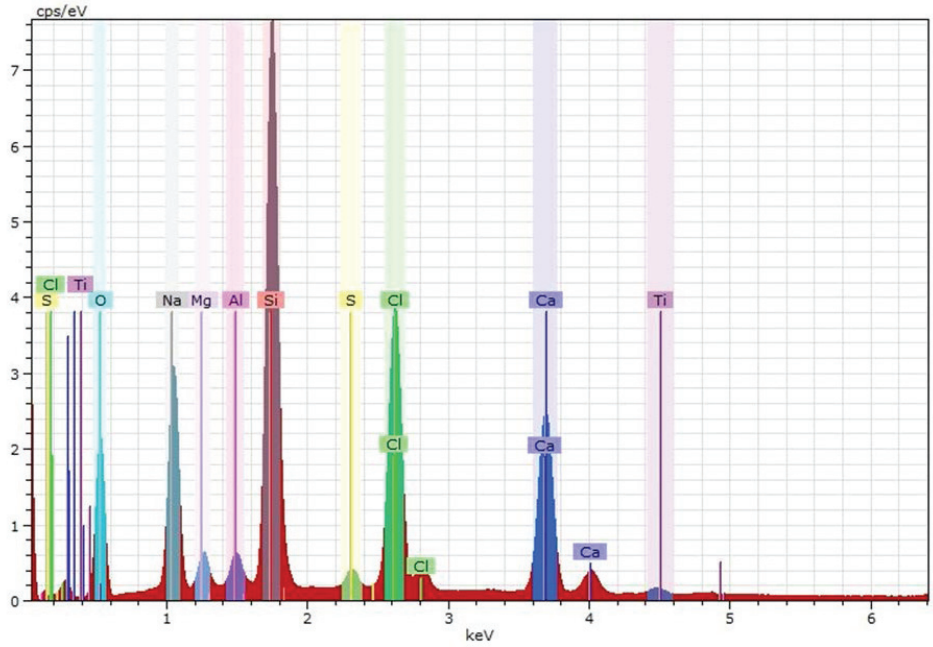

Fig. 11. Total EDX spectrum from the region of interest shown in Fig. 10; normalized counts per second versus energy (eV) of the detected X-rays.

3.2. Casing and Production string

The macroscopic images of the samples cored out from casing and production string from Ketzin Well 202 (Ktzi 202) are presented in Figs. 12 and 13. Rust layers were present at both internal (Fig. 12) and external (Fig.13) surfaces of production string (T) and casing (C) samples. Rust layers present on the internal side of the casings were thick and showed tendency to peel off. It was noticeably thicker than the rust layer on the production string. The rust spots on two uppermost production strings seemed to be aligned along a certain direction that could possibly be fluids flow direction in the production string. This alignment was not observed for the deepest production string sample T452. This alignment can either be associated with a mechanical abrasion upon fluid flow or direction specific rusting on CO_2 flow through the production string. The colour of rust at casings both internal and external sides was dominated by red-brown while the colour of production strings had admixtures of brown-black. The red-brown colour is characteristic for hematite while the black admixture may suggest presence of magnetite in corrosion products. The external production string surface was the darker the deeper in a well the sample was residing. The external surfaces of casings had a comparable colour and roughness regardless the depth they were retrieved from.

Figure 14 compares images taken at various surfaces for exemplary production string (T9) and casing (C19) samples at the same magnification (×40). The microscopic images showed a distinct difference between casing and production string interfaces. Generally the casing sample interfaces were more inhomogeneous and rough compared to production string interfaces. The higher roughness of the rust on the internal casing interfaces could have possibly been associated with higher corrosion degree at these interfaces.

Fig. 12. Images of internal surfaces of casing (C) and production string (T) samples retrieved at different depths.

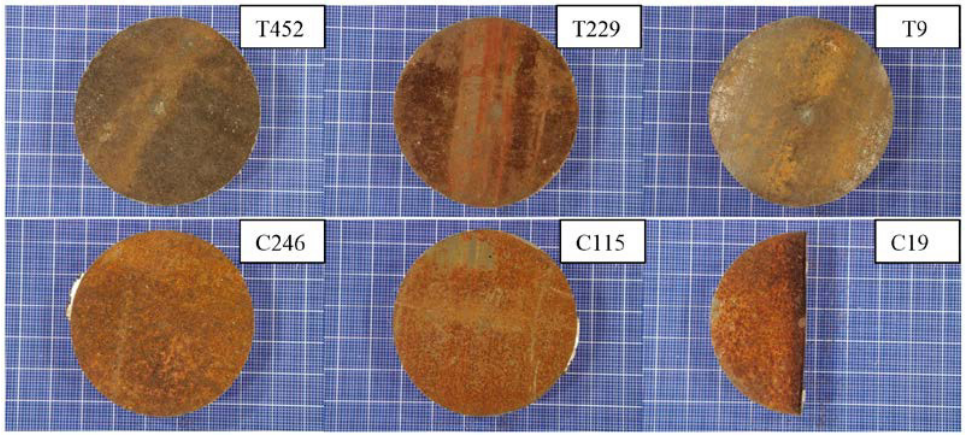

Fig. 13. Images of external surfaces of casing (C) and production string (T) samples retrieved at different depths.

Thickness of the internal and external rust layers for two exemplary samples T9 and C19 was estimated based on microscopic images (magnification ×7) for cross-sectioned samples. The samples for cross-section analysis were fixed by an epoxy resin prior to cutting. This prevented potential mechanical damages of the rust layers on cutting. The microscopic images of cross section surfaces are presented in Fig. 15. Figure 16 compares thickness of the rust layers at internal and external surfaces for exemplary production string (T9) and casing (C19) samples. The thickest layer of rust was present at internal casing surface. The average thickness estimated based on 13 random measurements was about 190 µm. In contrast to casing, the average thickness of the rust layer on the internal production string surface was the lowest and it was about 30 µm. The average thicknesses of the rust layers present at external surfaces of production string (T9) and casing (C19) were about 60 and 40 µm respectively.

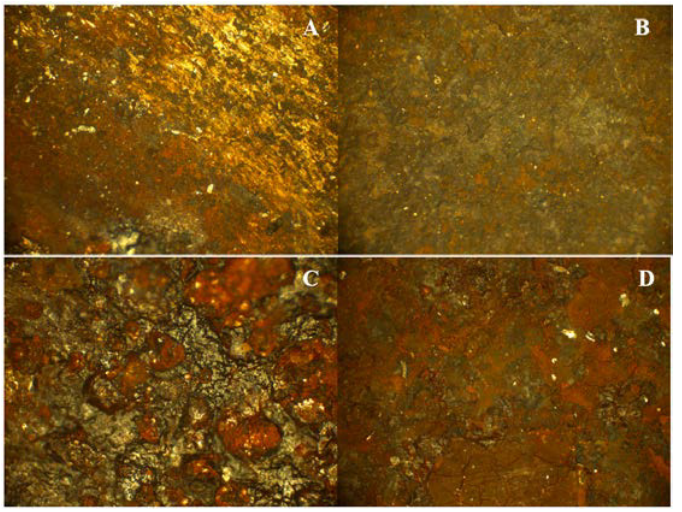

Fig. 14. Microscopic images (magnification ×40) of: production string T9 (top) inside (A) and outside (B) surfaces; casing C19 (bottom) inside (C) and outside (D) interfaces.

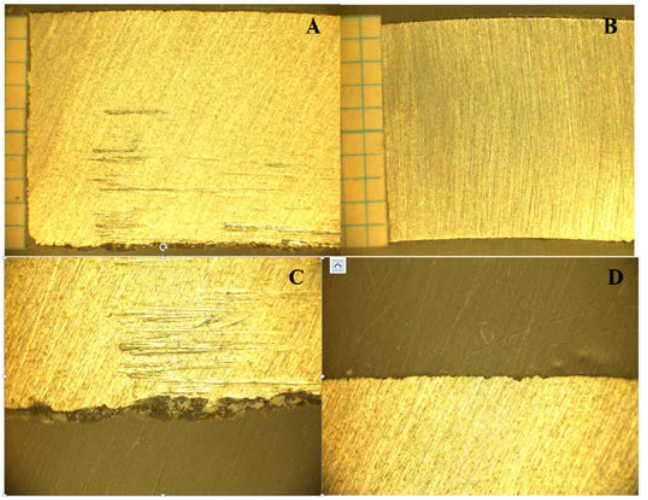

Fig. 15. Optical microscope images of cross-sectional surfaces of casing sample C19 (A) and production string (T9) taken at magnification 7 times and 10 times magnified internal (C) and external (D) rust layers at casing sample C19.

Fig. 17. presents the relation between the depth at which production string and casing samples were retrieved and the thickness of the rust layer present at the internal pipe surface. Both for casings and production strings the same trend was observed, namely increase in the rust layer thickness with the depth at which samples were residing. This effect may be associated with increasing temperature and pressure along with the depth in a well and thus enhanced corrosion as corrosion rates increases with temperature and pressure [11]. The thickness of the rust layer at casing strings was one order of magnitude higher than on production strings. While on production strings it was in the order of tens of micrometers, the rust thickness on casings was between 200 and 360 micrometers depending on depth. The values obtained for T9 and C19 samples using the dial indicator are in a very good agreement with the rust

thickness estimates using the microscopic based method. Although the respective analysis of the external surfaces was not conducted due to high measurement uncertainties at these surfaces, the visual observations (Fig. 13) suggest that the same relation between corrosion degree at the external production string surfaces and the production string depth applies.

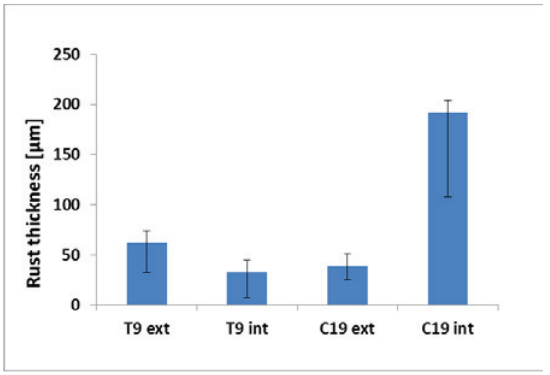

Fig. 16. Thickness of the rust layer estimated based on microscopic images at different surfaces for production string T9 and casing C19 samples.

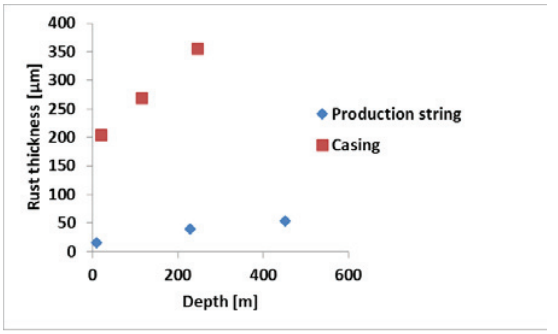

Fig. 17. Thickness of the rust layer at internal surface vs. depth of sample retrieval for casing and production string samples (based on dial indicator readings).

3.2.1. Video inspection of well Ketzin 202 in 2009 and 2011

Video inspection of the 5 ½" production string was performed in 2009 and 2011. A camera was descended all the way to the casing shoe while continuously filming. The camera was stopped at some depths to record the inner surface of the casing. The camera was in motion at the depths from which the casing samples were cored afterwards (8.8 m, 228.5 m and 452.2 m), so no images could be extracted for direct comparison. At about 300 m in 2009, and about 412.8 m in 2011, the camera dived into the brine. This reduced the quality of the recording. The intervals with the perforations (about 623.5 m – 632.5 m and 648.6 m – 652.3 m) were recorded in more detail and at lower speed. Bottom of the well was reached in 2009. In 2011, however, something blocked the borehole in the centre, and the camera could not descend beyond 652 m. Figures 18 and 19 show snapshots of the inner casing surface at several depths.

Already in 2009, some corrosion products were partly covering the casing surface at lower depths (Fig. 18 (a,b)). Below the depth of 300 m, the image quality was not sufficient to determine with certainty whether there were any corrosion products on the surface. Within the perforated interval, the casing surface was either fairly smooth or covered with presumably precipitates and/or corrosion products.

The recording from 2011 reveals that the upper most portion (down to about 100 m) of the production string had a significant amount of corrosion products on the surface (Fig. 19 (a,b)). Although the quality of the images was reduced with depth, especially below 412 m, it seems that there were smaller patches of corrosion products at greater depths. It is difficult to estimate the condition of the perforated intervals in 2011 based on the video only (unstable image).

The main conclusion from these video recordings is that the production string exhibited some degree of corrosion on the inner surface before the cement plug was set (2013) and long before the core samples were retrieved (2015). It is questionable to how much (surface coverage, thickness of corrosion products) has the corrosion progressed between 2009 and 2011, especially in the lower part of the well where the recordings were not so clear due to presence of brine. In any case, this excludes the possibility that the corrosion of the casings was entirely due to the pipes being exposed to ambient conditions at the Ketzin site after retrieval.

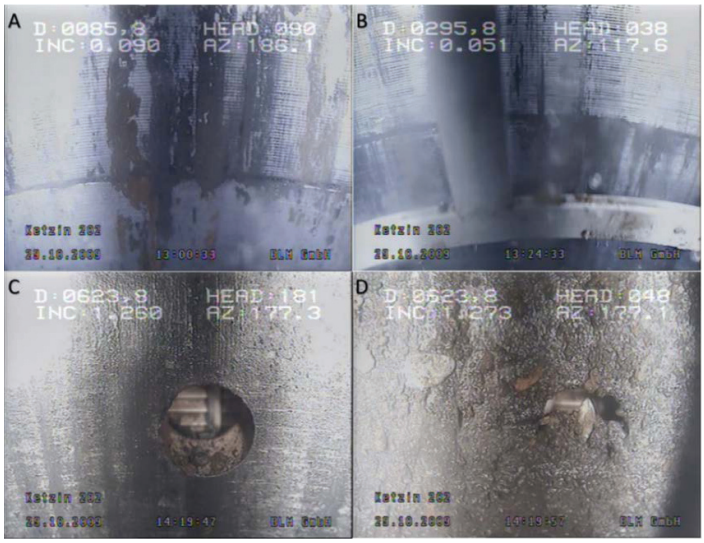

Fig. 18. Snapshots of the 5 ½" production string from 2009 at depths: (a) 85.8 m, (b) 295.8 m, (c) 623.8 m – a clean perforation, and (d) 623,8 m – a clogged perforation.

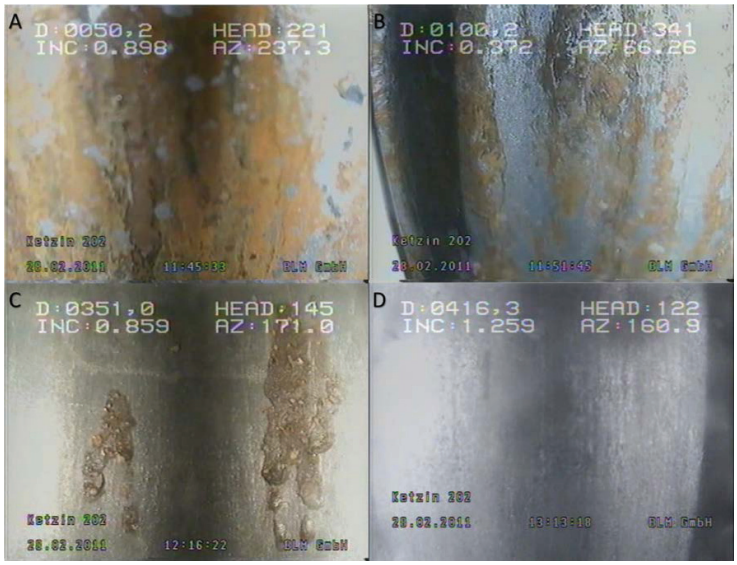

Fig. 19. Snapshots of the 5 ½" production string from 2011 at depths: (a) 50.2 m, (b) 100.2 m, (c) 351 m, and (d) 416.3 m.

4. Conclusions

X-ray computed tomography analysis supported by AVIZO 3D visualization showed difference in homogeneity of the cement material.

- The reference sample was homogeneous with some closed pores evenly distributed within the sample volume.
- The downhole samples had some voids unevenly distributed within volume.
- No correlation between the depth of the cement sample and the pore volume per sample was found.
- Two distinguishable cement materials were observed within the cement volume.
- EDX analysis of the two materials showed difference in their chemical composition. One of the materials was NaCl rich.

Three casing and three production string samples retrieved at different depths of Ketzin observation well 202 were analysed. Focus was on the degree of rusting.

- All steel surfaces showed some rusting, though the level of corrosion on the casings appear to be relatively low.
- Rust thicknesses on the internal surfaces of casings were one order of magnitude higher than rust thicknesses on production strings.
- Rust thickness on both casing and production string strings increased with depth.

Acknowledgements

Financial support for this work was from the Norwegian Gassnova-funded project "Improving CO_2 well integrity by studies of materials from Ketzin wells", which is an add-on to the German COMPLETE project which is funded by the Federal Ministry of Education and Research, OMV, RWE, Vattenfall, VGS and Statoil. We also acknowledge NTNU NanoLab and NTNU Institute of Physics for the use of their equipment.

References

[1] Martens S, Kempka T, Liebscher A, Lüth S, Möller F, Myrttinen A, Norden B, Schmidt-Hattenberger C, Zimmer M, Kühn M. Europe's longest-operating on-shore CO_2 storage site at Ketzin, Germany: A progress report after three years of injection. Environmenal Earth Science 2012; 67: 323-334. doi: 10.1007/s12665-012-1672-5.

[2] Martens S, Liebscher A, Möller F, Henninges J, Kempka T et al. CO_2 storage at the Ketzin pilot site: Fourth year of injection, monitoring, modelling and verification. Energy Procedia 2013; 37: 6434-6443. doi:10.1016/j.egypro.2013.06.573.

[3] Liebscher A, Möller F, Bannach A, Köhler S, Wiebach J, Schmidt-Hattenberger C, Weiner M, Pretschner C, Ebert K, Zemke J. Injection operation and operational pressure-temperature monitoring at the CO_2 storage pilot site Ketzin, Germany - Design, results, recommendations. International Journal of Greenhouse Gas Control 2013; 15: 163-173. doi:10.1016/j.ijggc.2013.02.019.

[4] Martens S, Moeller F, Streibel M, Liebscher A, the Ketzin Group. Completion of five years of safe CO_2 injection and transition to the post-closure phase at the Ketzin pilot site. Energy Procedia 2014; 59: 190-197.

[5] Prevedel B, Martens S, Norden B, Henninges J, Freifeld BM. Drilling and abandonment preparation of CO_2 storage wells – Experience from the Ketzin pilot site. Energy Procedia 2014; 63: 6067-6078.

[6] Eiken O, Ringrose P, Hermanrud C, Nazarian B, Torp TA, Høier L. Lessons Learned from 14 years of CCS Operations: Sleipner, In Salah and Snøhvit. Energy Procedia 2011; 4: 5541-5548.

[7] Carey JW, Wigand M, Chipera SJ, WoldeGabriel G, Pawar R, Wehner SC, Raines MA, Guthrie Jr GD. Analysis and performance of oil well cement with 30 years of CO_2 exposure from the SACROC Unit, West Texas, USA. International Journal of Greenhouse Gas Control 2007; 1(1): 75-85.

[8] Crow W, Carey JW, Gasda S, Brian Williams D, Celia M. Wellbore integrity analysis of a natural CO_2 producer. International Journal of Greenhouse Gas Control 2010; 4(2): 186-197.

[9] Scherer GW, Kutchko B, Thaulow N, Duguid A, Mook B. Characterization of cement from a well at Teapot Dome Oil Field: Implications for geological sequestration. International Journal of Greenhouse Gas Control 2011; 5(1): 115-124.

[10] Todorovic J, Torsæter M, Opedal N, Wiese B, Martens S. Characterization of CO_2 Pipeline material from the Ketzin pilot site. Energy Procedia 2014; 63: 2610-2621.

[11] Linda Garverick. Corrosion in the Petrochemical Industry. ASM International, Jan 1, 1994.